

## Diffusion of a test electron beam by a broad wave spectrum propagating in a traveling wave tube

F. Doveil, and D. Guyomarc'h

*Equipe Turbulence Plasma, PIIM,  
UMR 6633 CNRS-Université de Provence,  
Centre universitaire de Saint-Jérôme, service 321, F-13397 Marseille cedex 20*

The velocity diffusion of particles in a field of randomly phased waves is considered. An arbitrary waveform generator is used to launch a prescribed discrete spectrum of waves along the slow wave structure of a Traveling Wave Tube (TWT) [1]. A cold test electron beam propagates along the axis of the TWT and interacts with the waves whose power is much larger than the beam kinetic power. A trochoidal energy analyzer [1] records the beam energy distribution at the output of the TWT. The energy spread of the electron beam is measured as the position of the emitter probe along the TWT is varied. A velocity diffusion coefficient can thus be measured. Two different situations are compared: one with a large overlap parameter between neighboring modes where standard quasilinear diffusion theory is valid; and one with an intermediate overlap parameter where numerical simulations [2] have shown that the diffusion coefficient exceeds the quasilinear value by a factor of about 2.5.

The apparatus is shown schematically in Fig.1. It consists of a traveling wave tube modified so that either a cold or a warm beam interacts with the waves on the slow wave structure. The slow wave structure is made long enough to allow non linear processes to develop. It consists in a wire helix that is rigidly held together by three threaded alumina rods and is

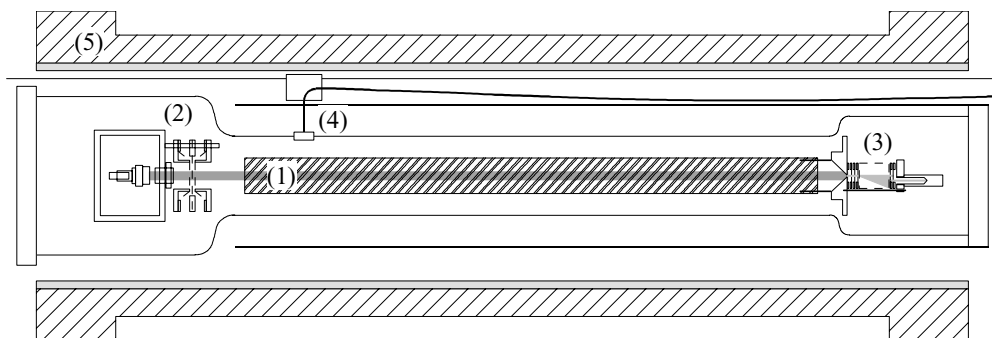


Fig.1 Sketch of the TWT : (1) helix, (2) electron gun and spreader, (3) trochoidal analyzer, (4) one of four axially movable probes, and (5) magnetic coil.

enclosed by a glass vacuum tube. The 4.0 m long helix is made of a 0.3 mm diameter Be-Cu wire ; its radius is 11.3 mm ; its pitch is 0.8 mm. The diameter of each alumina rod is 6 mm.

A resistive rf termination at each end of the helix serves to reduce reflections. The glass vacuum jacket is in turn enclosed by an axially slotted 5.75 cm radius cylinder that defines the rf ground. Inside this cylinder but outside the vacuum jacket are four axially movable probes which are capacitively coupled to the helix. The dispersion relation, shown on Fig.2, closely resembles that of a finite radius, finite temperature plasma. But, unlike a plasma, the helix does not introduce any appreciable noise. This allows to define

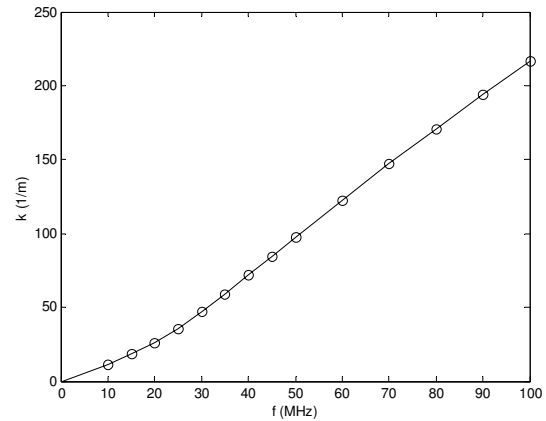


Fig.2 Dispersion relation of the helix

and control the input wave spectrum by launching a « repetitive noise » on one probe. We consider two different signals whose amplitudes spectra for the potential on the helix are

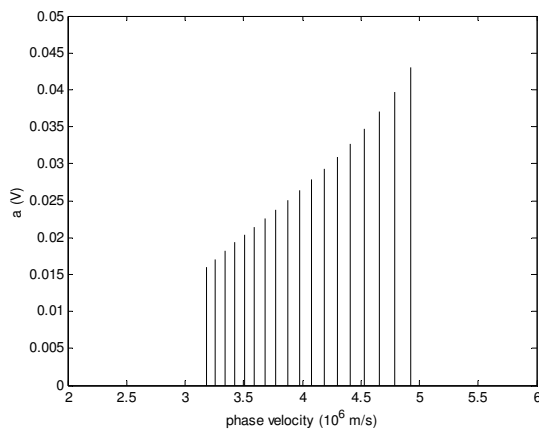


Fig.3a Wave spectrum on the helix  
S1 :  $s = 2.5$  ;  $D = 1.5 \cdot 10^{16} \text{ m}^2/\text{s}^3$ .

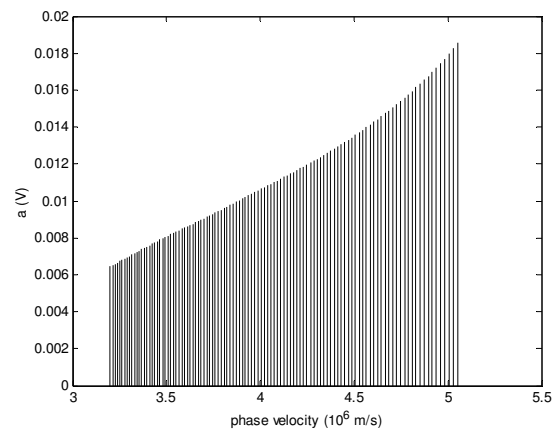


Fig.3b Wave spectrum on the helix  
S2 :  $s = 10$  ;  $D = 1.5 \cdot 10^{16} \text{ m}^2/\text{s}^3$ .

given on Fig.3. The phase of each mode is chosen randomly. For each mode, characterized by its frequency  $f$  (or related wavenumber  $k$ , or phase velocity  $v$ ) and amplitude  $a$ , one can define the overlap parameter  $s = 4 A^{1/2} / \Delta v$  and the quasilinear diffusion coefficient  $D = (\pi/2) A^2 k / \Delta v$ , where  $\Delta v$  is the phase velocity difference between two neighboring modes and  $A = \eta a$  with  $\eta = e/m$  ( $-e$  and  $m$  are the charge and mass of an electron). The amplitude spectrum S1 of Fig.3a (resp. S2 of Fig.3b) has been designed in such a way that, for every mode,  $s = Const. = 2.5$  (resp. 10) and  $D = Const. = 1.5 \cdot 10^{16} \text{ m}^2/\text{s}^3$ . As a result, the two spectra contain respectively 18 and 110 modes for a frequency ranging from approximately 20 to 50 MHz. Each spectrum is then normalized by the frequency dependent coupling

coefficient of the emitting probe in order to adjust the potential amplitude on the helix to the desired one.

The electron beam is produced at one end of the slow wave structure and is confined along the axis of the helical slow wave structure by a strong axial magnetic field (500 gauss). The central part of the electron gun consists of the grid-cathode subassembly of a ceramic microwave triode and the anode is replaced by a Cu plate with an on-axis hole whose aperture defines the beam diameter (5mm).

A trochoidal analyzer is set at the output of the slow wave structure. It works on the principle that charged particles undergo an  $E \times B$  drift when passing through a region in which an electric field  $E$  is perpendicular to a magnetic field  $B$ . Although the drift velocity is the same for all electrons, the total displacement is greater for slower electrons. Electrons that can escape the drift region are characterized by a specific energy  $w_p$  given by the dimensions of the analyzer and the amplitude of the electric and magnetic field [1].

The electron energy distribution is determined by retarding the electron beam by means of entrance electrodes and selecting electrons having the correct drift energy  $w_p$  determined by the potential difference on the deflector plates. A sketch of the trochoidal analyzer is shown in Fig.4. All electrodes of the system are made with a molybdenum annulus (external diameter 16 mm, internal diameter 8 mm) on which is sandwiched a thin stainless steel sheet with one or two apertures (diameters 0.5 and 1 mm and offset 3.2 mm). The

beam current is measured on the first electrode  $E_1$ . The retarding system consists of four electrodes  $E_1$  to  $E_4$  on which a retarding potential is equally distributed. It

is followed by two deflector plates  $D_1$  and  $D_2$  in the drift region (length 19 mm, gap 3.2 mm). Most of the electrons that have not been scattered are collected by electrode  $E_6$ . Finally scattered electrons are accelerated between electrodes  $E_5$  and  $E_6$  and collected in the Faraday cup located behind the off axis aperture in  $E_6$ . The current is measured by means of a picoammeter. Retarding potential and measured current are computer controlled allowing an easy acquisition and treatment.

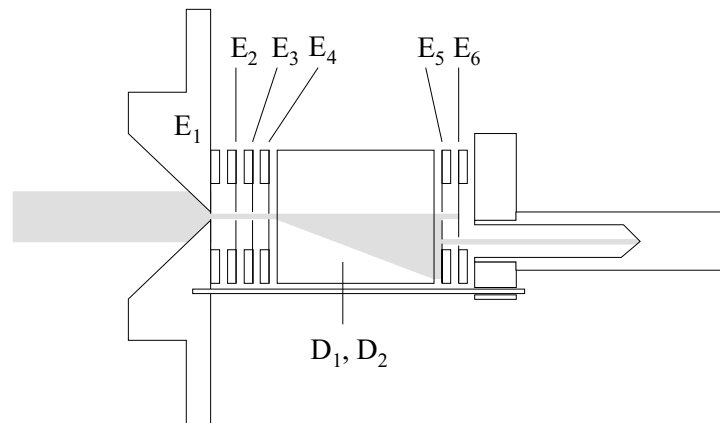


Fig.4 Sketch of the trochoidal analyzer

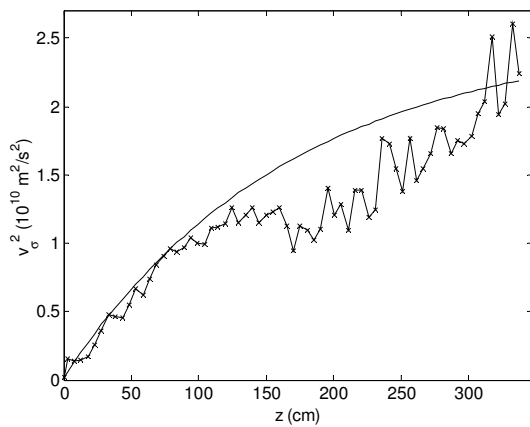


Fig.5a Beam velocity diffusion for spectrum S1

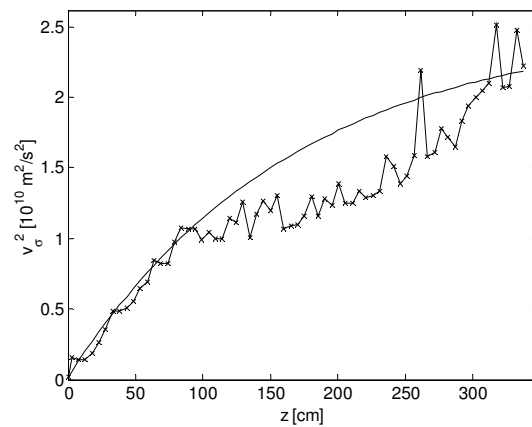


Fig.5b Beam velocity diffusion for spectrum S2

A weak cold beam, with energy  $E_b = 47\text{eV}$  and current  $I_b = 0.25\ \mu\text{A}$ , propagates along the axis of the TWT with a mean velocity  $v_b = 4 \cdot 10^6\ \text{m/s}$  located inside the phase velocity range of the “repetitive noises” of Fig.3. The position of the emitter probe used to launch the repetitive noise along the helix of the TWT is varied. As the emitter gets closer to the helix end, the resonant interaction length of the beam with the prescribed fluctuating electric field decreases. The launched wave power is much larger than the beam kinetic power, so that amplification of the waves by the test beam is negligible. For each emitter position, the average beam energy distribution given by the trochoidal analyzer is recorded. In all the cases, the measured beam distributions are well approximated by Gaussians, i.e.,  $\exp[-(v-v_0)^2 / (v_\sigma)^2]$ . Fig.5a gives the dependence of measured  $(v_\sigma)^2$  as a function of the emitter position for launched spectrum S1, while Fig.5b corresponds to launched spectrum S2. Both curves show a similar velocity diffusion of the beam. For comparison, the continuous curve gives the diffusion predicted by quasilinear theory when taking into account an average damping of the waves by the resistive helix ( $k_i = 0.3\ \text{/m}$ ). Numerical simulations [2] have shown that, in the case of spectrum S1 with overlap parameter  $s = 2.5$ , the diffusion coefficient exceeds the quasilinear by a factor of about 2.5 beyond the Dupree time. This time would correspond to a length  $l_D = v_b / (k^2 D/3)^{1/3} = 1.5\ \text{m}$  for the conditions of the reported experiment. No net deviation is observed beyond this value when the results of Fig.5a and b are compared. A detailed analysis of the experiment is necessary before the discrepancy between numerical simulations and experiment be explained.

#### References:

- [1] D. Guyomarc’h, and F. Doveil, Rev. Sci. Instrum. **71**, 4087 (2000).
- [2] J.R. Cary, D.F. Escande, and A. Verga, Phys. Rev. Lett. **65**, 3132 (1990).